Active Peptidic Mimics of the Second Intracellular Loop of the V_{1A} Vasopressin Receptor Are Structurally Related to the Second Intracellular Rhodopsin Loop: A Combined ^{1}H NMR and Biochemical Study†

Hélène Déméné,‡ Sébastien Granier,§ Dany Muller,§ Gilles Guillon,§ Marie-Noëlle Dufour,|| Marc-André Delsuc,‡ Marcel Hibert,⊥ Robert Pascal,||,@ and Christiane Mendre*,§

Centre de Biochimie Structurale, UMR 5048 CNRS-UM1/UMR 554 INSERM-UM1, 29, rue de Navacelles, 34060 Montpellier Cedex, Unité INSERM U469, CCIPE, 141 rue de la Cardonille, 34094 Montpellier, Unité CNRS UPR 2580, CCIPE, 141 rue de la Cardonille, 34094 Montpellier, and UMR 7081, Université Louis Pasteur, Faculté de Pharmacie, 67400 Illkirch, France

Received December 13, 2002; Revised Manuscript Received May 13, 2003

ABSTRACT: Vasopressin (VP) receptors belong to the widespread G protein-coupled receptor family. The crucial role of VP receptor intracellular loops in the coupling with the heterotrimeric G proteins was previously demonstrated by construction of a vasopressin receptor chimera. Yet, no fine structural data are available concerning the receptor molecular determinants involved in their interactions with G proteins. In this study, we synthesized both a linear and a cyclic form of the second intracellular loop (i2) of the human V_{1a} vasopressin receptor isoform that is important for the interaction between the αq/α11 G protein and the receptor. These two peptides are biologically active. They specifically inhibit vasopressin binding to the V_{1a} receptor, suggesting that the corresponding endogenous peptides contribute to the structure of the vasopressin binding site via intra- or intermolecular interactions with the core of the V_{1a} receptor. The i2 peptide structures were determined by ^{1}H NMR. Both exhibit a helix and helical elements in their N- and C-terminal parts, respectively, separated by a turn imposed by a proline residue. More interestingly, the central Pro-Leu motif conserved in many GPCRs and thought to be important for coupling to G proteins can adopt different conformations. The "U" shape structure of the i2 loop is compatible with its anchoring to transmembrane domains III and IV and is very similar to the shape of bovine rhodopsin i2. Altogether, these data contribute to a better understanding of the structure of a not yet crystallized GPCR using the mimetic peptide approach.

G protein-coupled receptors (GPCRs)[1] are expressed at the surface of cells and involved in the control of fundamental aspects of the behavior and physiology of living organisms, mediating signals from hormones, neurotransmitters, autocrine and paracrine factors, nucleotides and nucleosides, lipids, and proteins and having light, odorant, and taste-sensing functions. Association of GPCRs with their specific ligands is thought to trigger a conformational change, enabling them to interact with heterotrimeric G proteins (*1*). One of the greatest challenges in this research field is to characterize the GPCR structural determinants involved in the interaction with their partners and more particularly to understand the molecular basis of G protein selectivity. Relatively recently, Palczewski et al. (*2*) published the first high-resolution structure of a well-known GPCR, rhodopsin. While this study represents an important piece to the puzzle of GPCR-mediated signal transduction, the applicability of the rhodopsin paradigm to other GPCRs is questionable (*3*). In particular, the high level of amino acid sequence variability observed in the GPCR intracellular loops, known to interact with G proteins, suggests that the structure of these coupling interfaces may be dissimilar. Indeed, ^{1}H NMR structural investigations have recently shown that the cytoplasmic loops of the α2A adrenergic receptor (i2) (*4*), angiotensin receptor

† This work was supported by Grant PCV00-86 from the "Programme CNRS Physique Chimie du Vivant".

* To whom correspondence should be addressed: Unité INSERM U469, CCIPE, 141 rue de la Cardonille, 34094 Montpellier, France. Phone: +33-4 67 14 29 84. Fax: +33-4 67 54 24 32. E-mail: Christiane.Mendre@ccipe.cnrs.fr.

‡ UMR 5048 CNRS-UM1/UMR 554 INSERM-UM1.

§ Unité INSERM U469, CCIPE.

|| Unité CNRS UPR 2580, CCIPE.

⊥ Université Louis Pasteur.

@ Present address: UMR5073, Université Montpellier 2, CC017, Place E. Bataillon, 34095 Montpellier, France.

[1] Abbreviations: BOP, benzotriazol-1-yloxytris(dimethylamino)-phosphonium hexafluorophosphate; CD, circular dichroism; CHO, Chinese hamster ovary; COSY, correlation spectroscopy; DIC, *N*,*N*′-diisopropylcarbodiimide; DIEA, *N*-ethyldiisopropylamine; DMF, *N*,*N*-dimethylformamide; DPC, dodecylphosphocholine; EDT, ethanedithiol; Fmoc, fluoren-9-ylmethoxycarbonyl; G protein, GTP binding protein; GPCR, G protein-coupled receptor; h-V_{1a}-R, human vasopressin receptor subtype 1a; h-V_2-R, human vasopressin receptor subtype 2; HOBt, *N*-hydroxybenzotriazole; i2 and i3, second and third intracellular loops of GPCRs, respectively; IPs, inositol phosphates; $^3J_{HN\alpha}$, vicinal spin−spin coupling constants between the backbone amide proton and the α proton; NMR, nuclear magnetic resonance; NOE, nuclear Overhauser effect; NOESY, NOE spectroscopy; PLC-*β*, phospholipase C*β*; SDS, sodium dodecyl sulfate; TCEP, tris(carboxyethyl)phosphine; TFA, trifluoroacetic acid; TFE, 2,2,2-trifluoroethanol; TIS, triisopropylsilane; TM, transmembrane; TOCSY, total correlation spectroscopy; VP, vasopressin; TOWNY, TOCSY without NOESY.

10.1021/bi027358n CCC: $25.00
Published on Web 06/18/2003

(i3) (*5*), pheromone receptor (i3) (*6*), parathyroid receptor (i3) (*7*), and canabinoid receptor (i3) (*8*) adopt a conformation strikingly different from that of rhodopsin. At present, there are no clues about the origin of such dissimilarities, though they are likely to contribute to the selectivity of GPCR coupling to heterotrimeric G proteins. The vasopressin receptor isoforms represent good candidates for studying such coupling determinants. Whereas the different subtypes (V_{1a}, V_{1b}, and V_2) exhibit a high level of amino acid sequence homology (40−50%), they interact with different G proteins (Gq and Gs). The V_{1a} and V_{1b} receptors are specifically coupled to αq/α11 G proteins that in turn activate the phospholipase Cβ, leading to the production of inositol phosphates (IPs) and diacylglycerol. In contrast, the V_2 receptor is coupled to the Gαs protein and stimulates adenylyl cyclase activity involved in cAMP production. By analyzing the pharmacological and functional properties of $V_{1a}-V_2$ chimera receptors, Wess and collaborators demonstrated that the second intracellular loop of the V_{1a} receptor is crucial for PLC-β activation via the αq/α11 G protein and that the third intracellular loop of the V_2 receptor triggers adenylyl cyclase activation via the Gαs protein (*9*, *10*). These functional data strongly suggest the involvement of these intracellular loops in the respective recognition and activation of the corresponding G proteins.

To better understand the mechanisms of interaction between intracellular loops of VP receptors and heterotrimeric G proteins, we thus decided to analyze the structure of these loops using the mimetic peptide strategy. The validity of this experimental approach was recently demonstrated by Yeagle et al. (*11*). They synthesized the intracellular loops of the bovine rhodopsin protein and showed that their structures are very similar to those determined by Palczewski et al. for the native crystallized molecule. In this report, we present structural investigations concerning synthetic peptides mimicking the second intracellular loop of the human V_{1a} receptor (h-V_{1a}-R) and discuss their properties compared to those of other structurally characterized GPCR i2 loops.

MATERIALS AND METHODS

Chemicals. Tritiated [Arg^8]vasopressin (60 Ci/mmol) ([^{3}H]AVP) was obtained from NEN Life Science Products; OH-LVA, a specific V_{1a} vasopressin antagonist (2000 Ci/mol), was radioiodinated using the IODO-GEN technique as described previously (*12*, *13*). [Arg^8]Vasopressin was obtained from Bachem.

Peptide Synthesis. Peptides were synthesized using standard methods of solid-phase peptide synthesis. Alkylation of thiol groups with bromoacetamide and thioether chemoselective ligation and cyclization were carried out in buffered water under a nitrogen atmosphere. The products were purified by semipreparative HPLC on a Vydac C18 column with linear gradients of a mobile phase consisting of solutions A [0.1% (v/v) TFA in water] and B [0.1% (v/v) TFA in acetonitrile]. The purity and the structure of the peptides were checked by analytical HPLC and mass spectrometry (MALDI-TOF). The control peptide i2 ET_A (Asp182−Glu205 sequence derived from the intracellular part of the bovine endothelin A receptor) was synthesized with the standard automated solid-phase peptide synthesis procedures and characterized in the laboratory.

Chinese Hamster Ovary Cell Culture and Membrane Preparation. Membranes from CHO cell lines stably transfected with the human V_{1a} and V_2 receptors (h-V_{1a}-R and h-V_2-R, respectively) were prepared as previously described by Cotte et al. (*14*).

Binding Experiments. [^{3}H]AVP binding to plasma membrane preparations was performed as described previously (*15*). Briefly, membrane preparations (10 μg of protein/assay) were preincubated for 15 min at 37 °C in 150 μL of a buffer containing 50 mM Tris-HCl (pH 7.4), 0.15 mM $MgCl_2$, 1 mg/mL bovine serum albumin, and 0.1 mM phenylmethanesulfonyl fluoride with increasing amounts of vasopressin receptor intracellular loops. Then 1 nM [^{3}H]AVP (displacement binding experiments) or increasing amounts of [^{3}H]-AVP (saturation binding experiments) were added to the medium, and the mixture was incubated for an additional period of 60 min. An excess of unlabeled AVP (1 μM) was also added to the incubation medium to determine the level of nonspecific binding. The reaction was stopped by addition of 4 mL of cold washing solution [10 mM Tris-HCl (pH 7.4) and 3 mM $MgCl_2$], and the mixture was immediately filtered onto the Whatman glass fiber (0.8−1.2 μm) previously presoaked for 2 h with 10 mg/mL BSA. The filters were then rinsed three times with 4 mL of the washing solution, and the remaining radioactivity was measured by liquid scintillation spectrometry. The level of specific binding was calculated as the difference between the total and nonspecific values.

[^{125}I]OH-LVA binding was performed as described previously (*12*). Briefly, 1−2 μg of membranes was incubated with or without vasopressin receptor intracellular loops at 37 °C as described above except that [^{3}H]AVP was replaced with [^{125}I]OH-LVA. The concentration of [^{125}I]OH-LVA used in the displacement experiments was around 45 pM, a value corresponding to the K_d of this labeled analogue for h-V_{1a}-R (*12*). Radioactivity was measured using a γ counter. In these experiments, we explored a range of synthetic peptide concentrations from 0.3 to 10 μM where nonspecific binding was not significantly modified from control levels without peptide. Nonspecific binding represented 53 ± 3% of the total binding under these conditions (four distinct experiments each performed in triplicate). For higher mimetic peptide concentrations (30 μM), the level of nonspecific binding increased up to 68 ± 7% of the total level of binding. To avoid nonspecific effects, we thus decided to use peptide concentrations not higher than 10 μM in this study.

Circular Dichroism (CD) Measurements. Peptide CD spectra were recorded on a Jobin Yvon CD6 spectropolarimeter. The spectra were scanned at room temperature in a quartz optical cell with a path length of 0.03 cm. Baseline spectra for each solvent were obtained before the peptide spectra. Peptides were diluted to a concentration of 150 μM in 50 mM phosphate buffer (pH 6.4) containing either trifluoroethanol (TFE), sodium dodecyl sulfate (SDS), or dodecylphosphocholine (DPC) (100 equiv).

NMR Spectroscopy. The 600 and 400 Bruker AMX spectrometers were used to carry out all NMR experiments. Peptide concentrations were typically between 1 and 2 mM. All the experiments were carried out in the phase-sensitive mode in a States−TPPI fashion (*16*). NOESY spectra were recorded with mixing times of 100 and 200 ms. TOCSY spectra used a spin-locking field of 10 000 Hz for a total

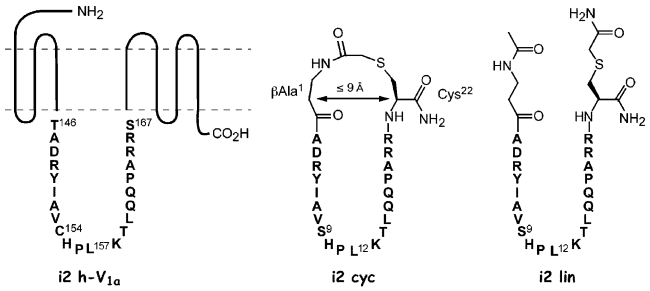

FIGURE 1: Sequence of the native second intracellular loop of the human V_{1a} vasopressin receptor (i2 h-V_{1a}-R) and structures of the cyclic (i2 cyc) and open chain (i2 lin) mimetic peptides. The *S*-carboxymethylcysteine-β-alanine linker of i2 cyc is suitable for reproducing a distance of up to 9 Å between the Cα atoms of βAla1 and Cys22 when completely extended.

duration of 40−60 ms, using a MLEV-17 or TOWNY (*17*) sequence. The typical spectral width was 6500 Hz in both dimensions, with 2048 data points in t_2 and 512 data points in t_1. Water suppression was achieved by application of a Watergate filter (*18*) or by presaturation of the water resonance during the relaxation delay (and mixing time for NOESY experiments). TOCSY and NOESY spectra were acquired at three temperatures (15, 20, and 30 °C) to alleviate resonance frequency overlaps. A phase-sensitive COSY spectrum helped us to discriminate Hα, Hβ, and Hγ resonances. Spectra were processed using the GIFA software (*19*). The two-dimensional matrices were multiplied by a shifted cosine-bell function, zero-filled to 512 × 1024 complex points, and Fourier transformed. Proton chemical shifts were referenced to internal H_2O.

Structure Calculations. Structure calculations were performed and NOE cross-peak assignments made in an iterative fashion using the Aria 1.1.2 module (*20*) implemented in CNS version 1.1 (*21*). Peak lists of the NOESY spectra with mixing times of 100 and 200 ms and chemical shift tables from Gifa (*19*) were used directly as input for Aria. The conversion from peak volumes to distances was done by Aria routines. For both peptides, the peak lists comprised approximately 10% of unassigned or partly assigned peaks. For example, for the i2 lin peptide, the HN resonances of Arg4, Tyr5, and Ala7 are very close and it is difficult to assign the relevant correlation peaks next to the diagonal in the HN/HN region. In a first step, we excluded all *unassigned* peaks that could have been interpreted as long-range constraints. These peaks were then manually assigned on the basis of the first calculated structures and reintroduced in the peak lists.

RESULTS

Design and Synthesis of the Linear and Cyclic Intracellular Loop of the V_{1a} Vasopressin Receptor. To synthesize a cyclic peptide mimicking the h-V_{1a}-R i2 loop (Figure 1), we used the h-V_{1a}-R model established by Phalipou et al. (*22*) to select the appropriate N- and C-terminal residues at the cytoplasmic ends of TM III and TM IV, respectively. We selected Thr146 and Ser167, corresponding putatively to a close contact (a 7.9 Å distance was evaluated between Cα atoms) and to an orientation compatible with side chain to side chain cyclization. A chemoselective ligation strategy was devised to synthesize a cyclic form (i2 cyc) of the peptide. Therefore, N- and C-terminal residues of the i2 loop were replaced with βAla and *S*-carboxymethylcysteine, respectively, to reproduce a distance similar to that evaluated from the h-V_{1a}-R model (Figure 1). Cys154 in the sequence of the receptor was also replaced with Ser9 in the peptide to avoid any possibility of incorrect cyclization. We also synthesized the linear peptide i2 lin which corresponds to the open chain form of the i2 cyc peptide.

Both peptides were obtained from resin-bound protected precursor **1**, which was prepared by solid-phase peptide synthesis using Fmoc chemistry (Figure 2). This precursor was either bromoacetylated, released from the solid support, and then subjected to a thioether chemoselective ligation (*23*) leading to the cyclic peptide i2 cyc, or alternatively, it was acetylated to give the linear model i2 lin after cleavage and alkylation with bromoacetamide (Figure 2). The intramolecular ligation of the linear peptide **2** was fast, compared to the bimolecular reaction of excess bromoacetamide with peptide **3**.

Biological Studies. Influence of h-V_{1a}-R i2 Loop-Derived Peptides on Radiolabeled Vasopressin Analogue Specific Binding to Human VP Receptors. The effects of i2 lin and i2 cyc were evaluated on their ability to alter the specific binding of either [^{3}H]AVP, a VP agonist, or [^{125}I]OH-LVA, a VP antagonist, on crude plasma membranes from CHO cell lines stably transfected with the human VP receptors. Between 0.3 and 10 μM, both i2 lin and i2 cyc dose-dependently inhibited the specific binding of [^{3}H]AVP to h-V_{1a}-R. i2 cyc mimetic peptide was found to be slightly more active than i2 lin. Maximal inhibitions observed at 10 μM were 62 ± 2 and 50 ± 4% for i2 cyc and i2 lin, respectively. This micromolar concentration range is consistent with values obtained with peptide segments derived from distinct receptors such as rhodopsin, α2A adrenergic, D1 dopamine, 5-HT-1A, V_{1a} vasopressin, or β2 adrenergic receptors (*24*−*29*). In contrast, used at the same concentration, these peptides were not able to inhibit [^{125}I]OH-LVA specific binding (Figure 3A).

Saturation experiments performed with [^{3}H]AVP in the presence or absence of 10 μM i2 cyc or i2 lin indicated that specific binding inhibition affected the maximal [^{3}H]AVP binding capacity (B_{max}) rather than the affinity (K_d) of the radiolabeled AVP for h-V_{1a}-R (data not shown), suggesting a noncompetitive inhibition mechanism.

To demonstrate the specificity of these effects, two control experiments were performed. First, we showed that a linear peptide i2 ET_A mimicking the second intracellular loop of the human endothelin A receptor was not able to inhibit the specific binding of [^{3}H]AVP to h-V_{1a}-R under experimental conditions where i2 cyc was active, i.e., 10 μM (Figure 3B). Second, we tested the influence of i2 lin or i2 cyc on the specific binding of [^{3}H]AVP to h-V_2-R, which belongs to the same GPCR family as h-V_{1a}-R. As illustrated in Figure 3B, even tested at 10 μM, i2 lin and i2 cyc did not alter the specific binding of [^{3}H]AVP to h-V_2-R.

CD Spectroscopy. To determine the secondary structure of i2 mimetic peptides, their CD spectra were recorded. In phosphate buffer alone, both peptides adopted a random conformation as indicated by a minimum of ellipticity observed at 198 nm (Figure 4A). The addition of 100 equiv of SDS (concentration higher than the critical micellar concentration) led to a slight right shift in the CD spectra, suggesting the presence of more secondary structure

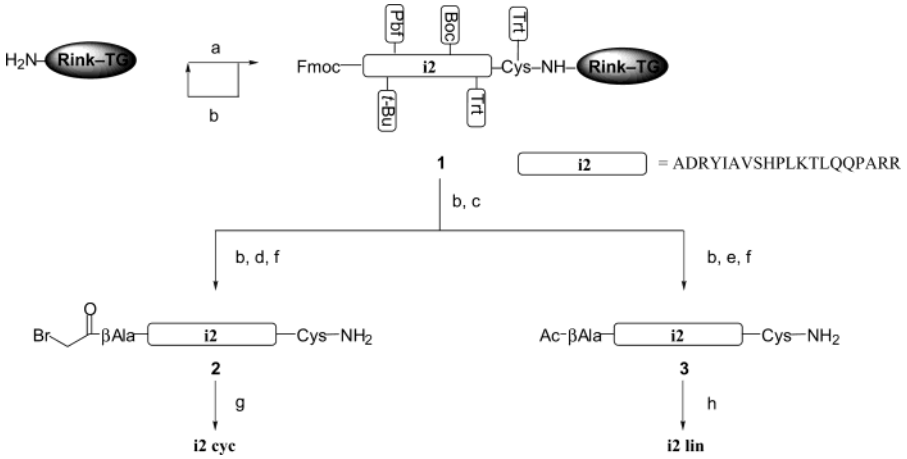

FIGURE 2: Synthesis of linear and cyclic i2 peptides: (a) Fmoc-Xaa-OH/DIC/HOBt, (b) piperidine/DMF (1:4, v/v), (c) Fmoc-βAla-OH/DIC//HOBt, (d) $(BrCH_2CO)_2O$, (e) Ac_2O, (f) TFA/H_2O/TIS/EDT (92.5:2.5:2.5:2.5, v/v/v/v), (g) 10^{-4} M, 2 h in Na_2HPO_4/NaH_2PO_4 buffer, TCEP (2.5 equiv at 30 min), and (h) $BrCH_2CONH_2$ (2.25 equiv), 20 h in Na_2HPO_4/NaH_2PO_4 buffer, TCEP (2.5 equiv).

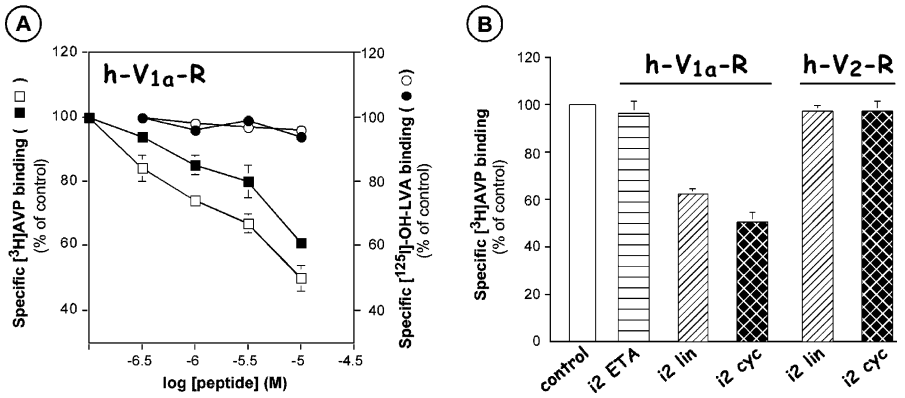

FIGURE 3: Biological properties of i2 mimetic peptides. (A) Influence of i2 mimetic peptides on specific binding of radiolabeled vasopressin analogues to human vasopressin receptors. Membranes from CHO cells which stably expressed h-V_{1a}-R (10 μg of protein/assay) were preincubated for 15 min without (control) or with increasing amounts of i2 cyc (□) or i2 lin (■) as described in Materials and Methods. Then 1 nM [^{3}H]AVP (total binding) or 1 nM [^{3}H]AVP with 1 μM unlabeled AVP (nonspecific binding) was added to the incubation medium and the reaction allowed to proceed for an additional 60 min. Levels of specific binding were calculated under each experimental condition and expressed as a percentage of control values (100% = 222 ± 8 dpm). Results are means ± the standard error of the mean of triplicate determinations from four independent experiments. Similar experiments with i2 cyc (○) or i2 lin (●) were performed using 45 pM [^{125}I]OH-LVA as radioligand. The level of specific binding was calculated and expressed as a percentage of control values (100% = 4400 ± 132 dpm). Results are means ± the standard error of the mean of triplicate determinations from three independent experiments. When no error bar is shown, it is smaller than the size of the symbol. (B) Specificity of i2 mimetic peptides on vasopressin receptor binding. Binding experiments were performed as described for panel A with CHO membranes which stably expressed h-V_{1a}-R or h-V_2-R with 1 nM [^{3}H]AVP in the presence or absence (control) of i2 lin, i2 cyc, or i2 ET_A (a synthetic peptide mimicking the intracellular loop of the i2 human endothelin A receptor). The level of specific binding was calculated and expressed as a percentage of control values (100% = 222 ± 8 dpm for CHO-h-V_{1a} and 382 ± 15 dpm for CHO-h-V_2-R). Results are means of triplicate determinations from three distinct experiments.

elements. In contrast, 100 equiv of DPC, added in the phosphate buffer, did not produce any more significant peptide structure modifications than the phosphate buffer alone (data not shown).

CD spectra exhibiting more typical features of helical elements (ellipticity minima at 206 and 224 nm) were obtained by adding TFE in the peptide dilution buffer. Titration experiments indicated that the maximum of secondary structure is obtained at a 50:50 ratio at room temperature (data not shown). Thus, further mimetic peptide structure investigations were performed under this last experimental condition.

NMR Structural Parameters. The structure of i2 lin and i2 cyc in 100% H_2O and a 50:50 TFE/H_2O mixture was studied by ^{1}H NMR at 400 and 600 MHz, respectively. We carried out the sequential assignment of all proton resonances following the standard method proposed by Wüthrich (*30*). The spectra of both peptides in pure water are typical of random coil averaged conformations (data not shown). In contrast, in accordance with the study by CD, addition of TFE causes a dispersion of proton resonances indicative of peptide folding in this solvent. Assignments of both peptides are listed in Table S1 of the Supporting Information. For both the linear and cyclic peptides, in the 50:50 TFE/H_2O buffer, the resonances of Leu12 are broad, which suggests a conformational exchange for this particular residue. For the linear peptide, after a careful inspection of the spectra, we have found a second HN resonance at 7.99 ppm. This second resonance, with a narrower line width, is of approximately the same intensity and exhibits an exchange peak on the NOESY spectra with the other resonance (Figure S1 of the Supporting Information). The broadening of the resonances is temperature-dependent, supporting the hypothesis of conformational exchange (Figure S2 of the Supporting

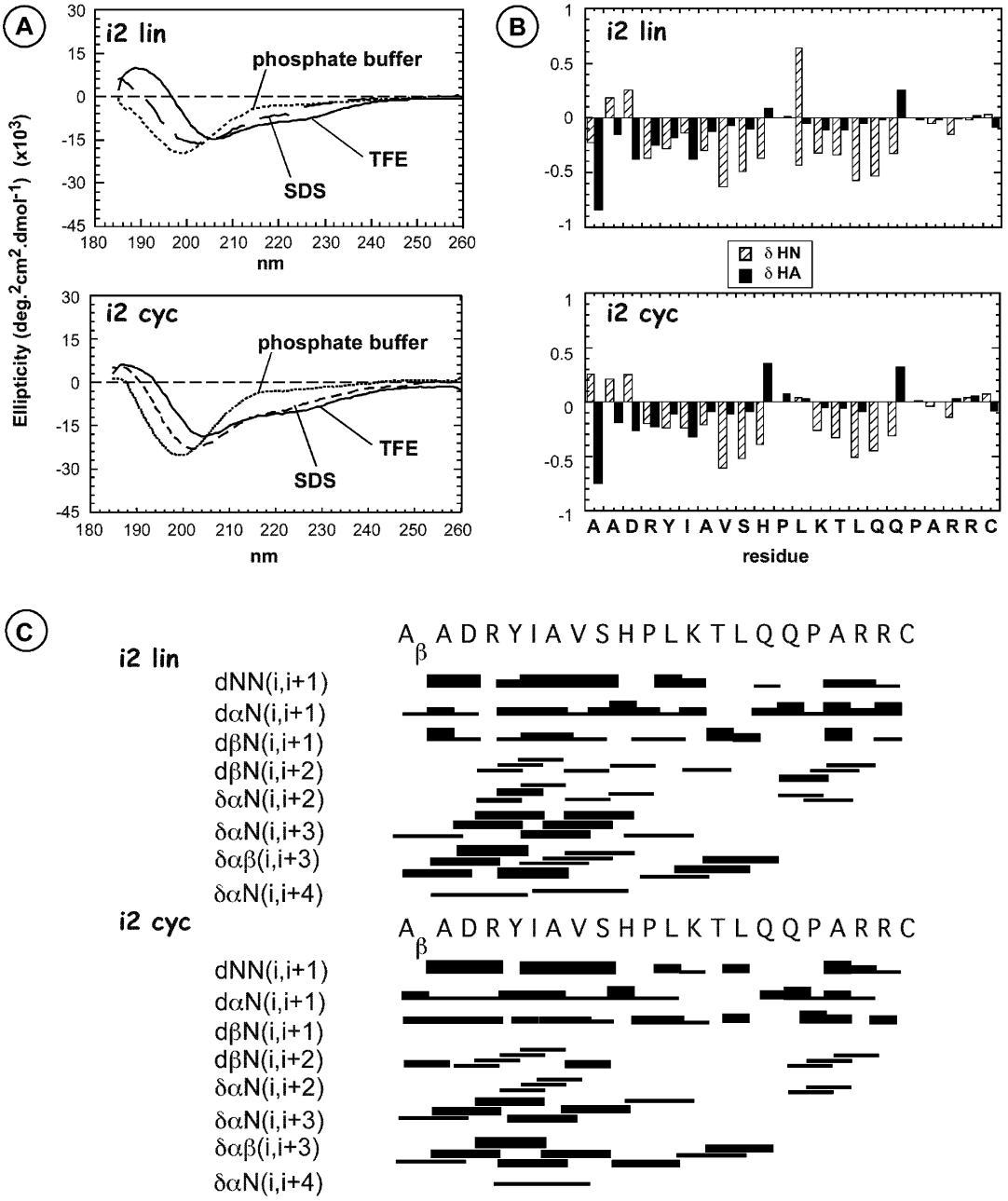

FIGURE 4: Structural properties of i2 mimetic peptides. (A) CD spectra of i2 lin and i2 cyc in phosphate buffer, in a phosphate buffer/TFE mixture (1:1, v/v), and in the presence of SDS micelles. The peptide concentration was 150 μM, and the SDS:peptide ratio was 100. (B) Plot of the deviations of HN and Hα chemical shifts (NMR) from random coil values for i2 lin (top) and i2 cyc (bottom). (C) Summary of the sequential and medium-range NOEs (NMR) for i2 lin (top) and i2 cyc (bottom) peptides. The thickness of the bars corresponds to the intensity of the NOEs.

Information). A possible explanation would be that this doubling of resonances is a result of a *cis*−*trans* equilibrium of the peptidic bond of Pro11. However, on the NOESY spectra, we could find no evidence of the presence of this equilibrium, such as concomitant αH His10−αH Pro11 and αH His10−*δ*H Pro11 NOEs. All the sequential NOEs between His10 and Pro11 indicate that the peptidic bond between His10 and Pro11 is *trans*. In addition, no second set of resonances was found for the adjacent residues. Finally, the presence of exchange peaks between the two resonances has not been reported to our knowledge for any *cis*−*trans* equilibrium in a peptidic bond. Hence, we conclude that the doubling of resonances for the amide proton of Leu12 originates from a conformational equilibrium that is not due to *cis*−*trans* isomerization of Pro11. Interestingly, this second amide resonance exhibits a pattern of additional middle-range NOEs peaks, namely, HN Leu12−Hβ Ala7 and HN Leu12−Hγ Gln16, that were not found for the resonances at 9 ppm (Figure S1 of the Supporting Information). The sequential and middle-range NOEs between Leu12 on one side and Pro11 and His10 on the other side show slightly reduced and increased intensities, respectively. Finally, the temperature dependence of the resonances at 9 and 7.99 ppm are +2.4 and −6.7 ppb/K, respectively, suggesting different levels of solvent exposure for the HN atom of Leu12 in the two conformations.

No second resonance was found for the cyclic peptide. The resonance of Leu12 for this closed form is found at 8.49 ppm, thus exactly the average between the two resonances observed for the linear peptide. Furthermore, it has a

Table 1: Structural Statistics Calculated for the 10 Low-Energy Structures Obtained for the i2 lin[a] and i2 cyc Peptides

	i2 lin	i2 cyc
no. of NOE restraints		
intraresidual	391 (*391*)	319
sequential	179 (*179*)	156
middle-range	194 (*194*)	137
long-range ($\|i - j\| > 4$)	6 (*8*)	19
rms deviations from experimental NOE restraints (Å)	0.067 ± 0.013 (0.080 ± 0.021)	0.081 ± 0.019
structural quality and coordinate precision		
backbone atom rmsd from mean (Å), residues 2−19	0.46 ± 0.19 (1.0 ± 0.37)	0.50 ± 0.10
heavy atom rmsd from the mean (Å), residues 2−19	1.22 ± 0.25 (1.410 ± 0.448)	1.33 ± 0.12
Ramachadran plot[b] (%)		
core regions	71.1 (*73.5*)	78.3
most favored regions	28.8 (*26.5*)	17.2
generously allowed regions	0 (*0*)	4.4
disallowed regions	0 (*0*)	0

[a] Calculated data corresponding to the conformation of the most shielded resonance of Leu12 for i2 lin are in italics. [b] Calculated with the program PROCHECK (*50*).

considerably larger line width than the other amide resonances. This suggests that we are in the presence of intermediate exchange between the two conformations observed on the spectra of i2 lin. No NOE was observed between this averaged resonance and the resonances of Ala7 and Gln16, but this does not invalidate our hypothesis as the complexity of dynamical parameters in the case of intermediate exchange makes the prediction of the presence or absence of NOEs difficult.

A source of information about protein secondary structure elements results from observed Hα and, to a less extent, HN chemical shifts when these are compared with random coil values. Three adjacent amino acids showing downfield changes (positive values) of more than 0.1 ppm indicate the presence of a stable β-structure, while three residues with negative changes of more than 0.1 ppm point to a well-defined helical structure (*31*). The differences in the HN and Hα chemical shift of linear and cyclic i2 loops between pure buffer and the 50:50 TFE mixture are depicted in Figure 4B. For both peptides, values suggesting the presence of helical elements in the N-terminal part (Asp3−His10) and to a lesser extent in the middle part (Lys13−Gln17) are observed. Pro11 is situated exactly between these two segments and most probably acts as a breaker of the regular secondary structure. Interestingly, for both peptides, the extreme N- and C-terminal parts exhibit similar behaviors; the residues in this C-terminal part are characterized by chemical shifts typical for random coil structures, whereas the residues in the N-terminal part are characterized by similar atypical value patterns. The incidence of cyclization upon the structure of the i2 loop can thus hardly be deduced from the chemical shift values of both peptides.

The presence of similar sequential and medium-range NOEs between both peptides (Figure 4C) supports this idea. Most of the differences in the (i, $i + 2$) and (i, $i + 3$) constraints could be assigned to superposition of NOEs in the corresponding peaks. An almost continuous stretch of sequential N_i−N_{i+1} NOEs interrupted by Pro11 and Pro18 is observed from the N- to the C-terminal part of both peptides, supporting indeed the existence of a helical conformation broken by the two prolines. The numerous medium-range i−$i + 2$ and i−$i + 3$ connectivities for the N-terminal part of both peptides validate the presence of helices for the N-terminal parts. The central and C-terminal parts also exhibit a few NOEs characteristic of helical elements, suggesting at least the presence of turns. In addition, Hβ Cys22−HN Asp3 , Hβ Cys22−HN βAla1, *S*-carboxymethyl Cys22 S-CH_2-CO proton−HN βAla1 (Figure 1), Hα Arg21−HN βAla1, and Hα Cys22−HN Ala1 NOEs are observed on i2 cyc NOESY spectra (data not shown). These NOEs are specific and characteristic of the cyclic structure of i2 cyc. In addition to these long-range NOEs specific to the cyclic peptide, a few long-range NOEs were found for the i2 lin and i2 cyc peptides: HN Ala7−Hβ Gln16, HN Ala7−Hγ Gln16, HN Ala7−Hα Gln16, Hδ Arg4−Hβ Lys13, Hγ Arg4−Hε Gln17, and Hβ Arg4−Hε Gln17. The aliphatic region is crowded for both peptides, and it may have prevented us from identifying more nonambiguous long-range constraints.

NMR Structures of i2 lin and i2 cyc Peptides. For both peptides, we were able to collect sufficient NOE distance constraints to calculate high-quality three-dimensional structures with the computer programs Aria and CNS. The best conformers are superimposed in Figure 5A, and Table 1 lists the structural statistics. For all structures, the backbone dihedral angles lie in the most favored regions of the Ramachandran map. For both peptides, the structure is characterized by the presence of a helix in the N-terminal part (residues 4−9), followed by a β-turn at the level of His10 and Pro11, a short step of 3-10-helix (residues 12−15), and a succession of turns in residues 16−20. The global fold of the peptides resembles a "U" with two arms constituted by the βAla1−Ser9 and Lys13−Cys22 segments and the bottom base by the His10−Leu12 stretch. The structures seem rather compact despite the paucity of long-range NOEs (i/j, $j > i + 4$), and we have thus repeated the calculations without them to investigate the contribution of these NOEs to the calculated fold (Figure S3 of the Supporting Information). The resulting structures are, as expected, slightly less compact, but the overall fold of the U shape is completely preserved. This can be attributed to the numerous i/j, $j = i + 4$ NOEs that unambiguously define the turns of the structure. The U-shaped structures are stabilized by a common network of hydrogen bonds: HN Ala7···CO Asp3, HN Ser9···CO Ser5, HN His10···CO Ile6, HN Thr14···CO Leu12, and HN Glu16···CO Lys13. The N-terminal helix in i2 cyc appears to be slightly more packed than in i2 lin due to cyclization. As a result, the CO group of Asp3 is engaged in a hydrogen bond with the HN atoms of Asp1 and Ala7 in i2 cyc, whereas a hydrogen bond between the CO group of Tyr5 and the HN atom of Val8 is observed in i2 lin.

The alternate conformation observed on the NMR spectra of the linear peptide is purely local at the level of the Pro11-Leu12 dipeptide. The transformation from one conformation to the other is of the "crankshaft" motion type (*32*−*36*) so that the Cα atoms of Pro11 and Leu12 remain at almost identical positions and the global fold of the linear peptide is completely preserved. This peculiar feature explains why the doubling of resonance was observed only for Leu12. Interestingly, the amide nitrogen atom of Leu12 is less exposed to the solvent in this alternate conformation, and its spatial position is now compatible with giving a hydrogen

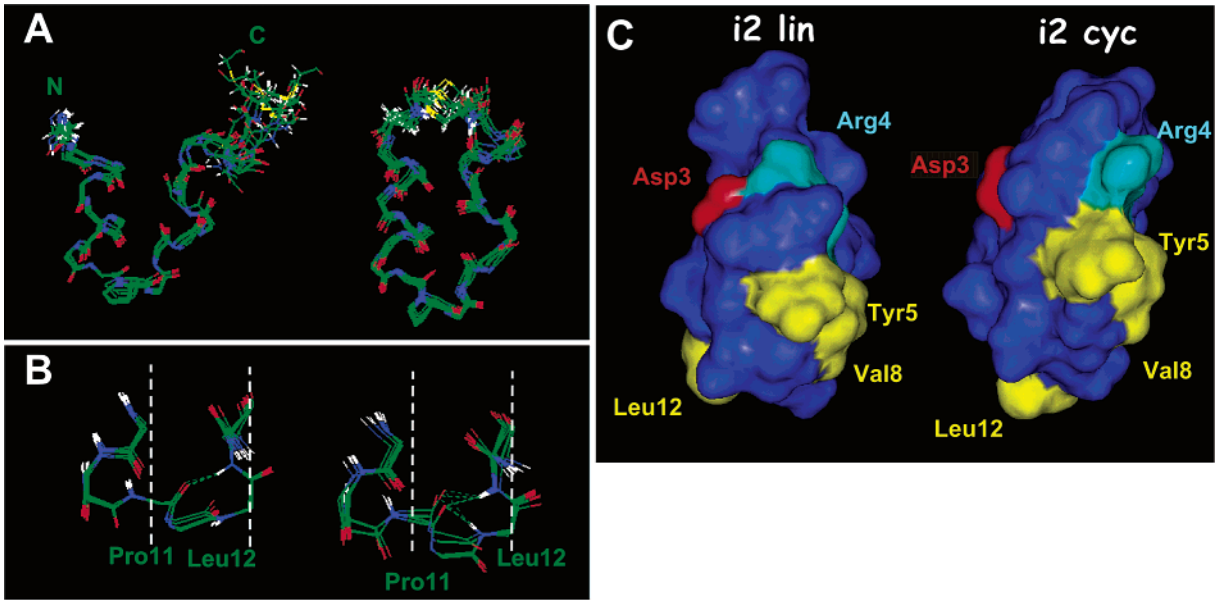

FIGURE 5: (A) Superposition of the 10 best conformers of i2 lin and i2 cyc calculated with Aria version 1.1. For clarity, only the backbone atoms are represented except for Pro11 where the side chain is represented. The conformers for the linear form are those calculated with the more deshielded resonance of Leu12 (no long-range NOE). The atoms are color-coded: white for hydrogens, red for oxygens, blue for nitrogens, green for carbons, and yellow for sulfurs. For the linear peptide, N- and C-terminal parts are identified with bold letters. (B) Local comparison of the 10 best conformers obtained with the two NMR constraint data sets for the linear forms. On the left are conformers calculated with the constraints of the more deshielded resonance of Leu12. On the right are conformers calculated with the constraints of the more shielded resonance of Leu12. The two conformers are related by a crankshaft motion so that the sum of the dihedral angles, $\psi^{11} + \phi^{12}$, is constant (*32*−*36*). The difference in the conformation is thus purely local at the dipeptide level, and the positions of Cα atoms of Pro11 and Leu12 remain unchanged between the two forms. Only atoms between the two dashed white lines drawn at the level of the $C\alpha^{11}$ and $C\alpha^{12}$ atoms occupy different positions in both conformers. The hydrogen bonds calculated with the "Insight" program are represented by green dashed lines. In addition to the amide proton of Lys13, the amide atom of Leu12 appears to be hydrogen bonded with the carboxyl oxygen atom of His10 in the conformations calculated with the constraints involving the shielded resonance of Leu12. (C) Surface representation of the mean structure of i2 lin and i2 cyc. Side chains of residues previously shown to be important for coupling with Gq proteins are colored yellow (hydrophobic residues), light blue (basic residues), and red (acidic residues).

bond with the carboxyl oxygen of His10 (Figure 5B). Although the temperature coefficient of the "alternate" resonance of Leu12 is not in favor of the existence of this hydrogen bond, it could explain the considerable difference in chemical shift for this residue between the two HN resonances measured on the spectra (1 ppm).

Figure 5C depicts a surface representation of the i2 lin and i2 cyc peptides. Colored (light blue, red, yellow, and green) residues correspond to residues that have been shown to be important for biological activity such as Asp3 (*37*), Glu4 (*37*), Tyr5 (*37*), Val8 (*37*), and Leu12 (*37*, *38*) in other Gq-coupled receptors. The helical conformation orients all these residues but Leu12 on the same face of the molecule, forming a potential intra- or intermolecular interaction surface. This was predicted by the mutagenesis studies carried out by Yamashita et al. on rhodopsin (*39*). Asp3 lies slightly apart, especially in the i2 cyc peptide as a byproduct from cyclization.

Comparison of the Global Folds of i2 lin, i2 cyc, and the Second Intracellular Loop of Bovine Rhodopsin. The hairpin-like structure of both peptides is reminiscent of the L shape of the second cytoplasmic loop in rhodopsin (*2*). Figure 6A represents a comparison of the global folds for all peptides. The N-terminal parts are likewise constituted by a short helix followed by a β-turn. The main differences are located in the C-terminal part, which appears to be more extended in the rhodopsin structure. Superposition of backbone atoms for the Ala2−Leu12 segment in the vasopressin peptides and the Ala132−Met143 segment in native rhodopsin yields indeed rms deviations of 2.2 and 1.7 Å^2 for the linear and cyclic peptides, respectively. The bottom base of the L loop is two residues shorter in the rhodopsin loop than in the i2 vasopressin loop. The main distance between both arms, as measured by the distance between the Cα atoms of βAla1 and Cys22, is 17.3 ± 1.6 and 6.9 ± 0.3 Å in i2 lin and i2 cyc, respectively. The corresponding distance in the rhodopsin structure is 12.8 Å. As evidenced by Figure 6A, the C-terminal part of the loops, which corresponds to the beginning of the transmembrane helix IV, is positioned identically in the cyclic peptide and in the rhodopsin structures. This suggests that the cyclization performed on the i2 vasopressin loop induces a structure very close to the native rhodopsin structure *in vivo*.

DISCUSSION

Although the high-resolution structure of bovine rhodopsin has been published relatively recently (*2*), structural data allowing a better understanding of how GPCRs mediate heterotrimeric G protein activation are still missing because of difficulties in obtaining crystals of purified hormone receptors. To circumvent these problems, we have adopted the mimetic peptide approach to study the structure of the second intracellular loop of h-V_{1a}-R known to be important for G protein coupling. Numerous studies, including one on rhodopsin, have used this approach facing the difficulties of production, folding, and crystallization of these proteins (*4*−*8*, *11*, *40*).

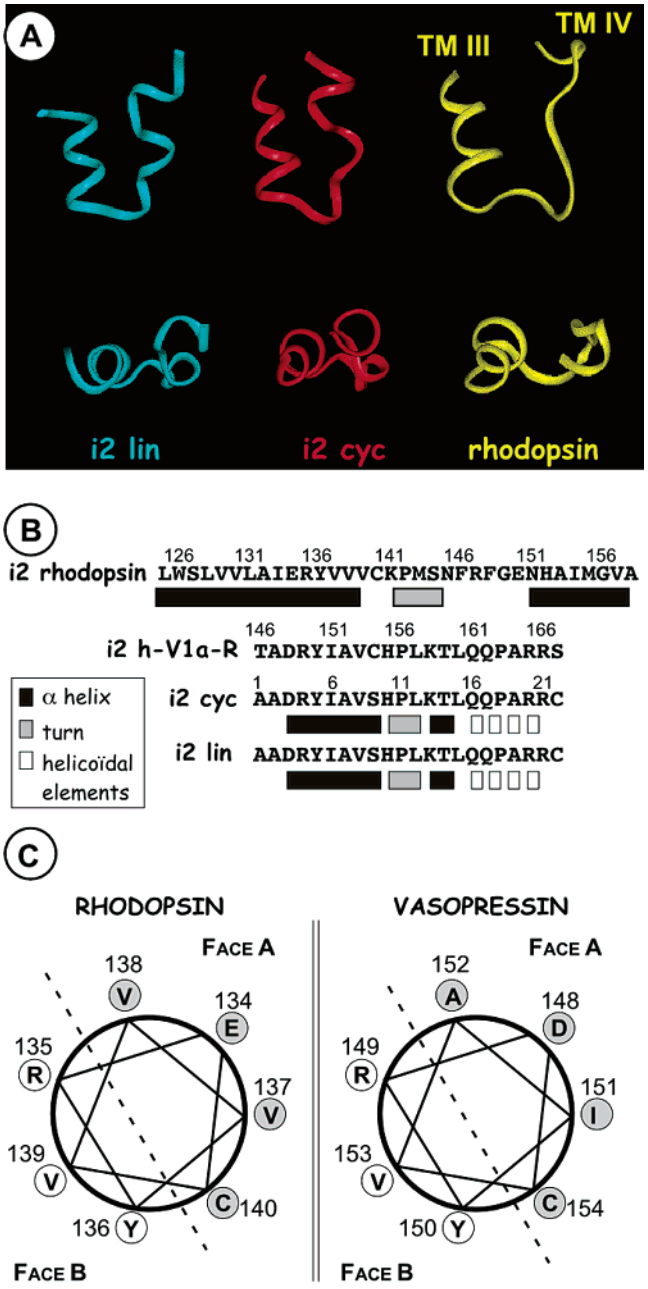

FIGURE 6: (A) Comparison of the backbone fold observed in i2 lin (blue), i2 cyc (red), and rhodopsin (yellow). The bottom structures are rotated 90° with respect to the top structures. (B) Comparison of the sequences and secondary structures in i2 lin, i2 cyc, and rhodopsin. (C) Comparison of the hydropathy profiles of the N-terminal segment of the second cytoplasmic loop of bovine rhodopsin and the V_{1a} vasopressin receptor.

In this study, the i2 mimetic peptides were synthesized as a linear or cyclic form. These peptides dose-dependently inhibit [^{3}H]AVP specific binding on a CHO cell line stably transfected with h-V_{1a}-R in a noncompetitive way. These peptide effects are (i) agonist specific since the specific binding of [^{125}I]OH-LVA, a specific V_{1a} vasopressin antagonist, is not affected, (ii) receptor subtype specific since no significant inhibition of specific binding of [^{3}H]AVP to h-V_2-R, a GPCR belonging to the same GPCR family, is detected up to 10^{-4} M, and (iii) sequence specific since a peptide derived from the second intracellular loop of the human endothelin receptor type A, also coupled to Gq, does not inhibit the specific vasopressin binding to h-V_{1a}-R. We suppose that the i2 peptides disrupt intramolecular interactions between the native h-V_{1a}-R i2 loop and another receptor region leading to a misfolded binding site or an unliganded receptor state.

The i2 mimetic peptides both exhibit a constrained structure as revealed by the CD and ^{1}H NMR study. In organic solvent, they present a U-shaped structure characterized by an α-helix in the N-terminal part, a turn imposed by the proline residue in the middle of the loop and helical elements in the C-terminal region (Figure 5A). The structure seems to be mainly determined by the amino acid sequence of the i2 loop since both the cyclic and linear peptides exhibit a similar molecular arrangement. Similarly, peptides corresponding to the cytoplasmic loops of rhodopsin have been shown to present turns independently of the membrane protein remainder (*11*, *40*, *41*). The biological relevance of a peptide structure determined in a TFE/H_2O mixture may, however, seem debatable. We emphasize that all secondary elements observed in the U-shaped structure were already observed in a 10:90 TFE/H_2O mixture at 10 °C (Figure S4 of the Supporting Information). To study by NMR membrane-associated peptides, one has to resort to membrane-mimicking solvents, such as TFE, or to small detergent micelles. Recent studies have highlighted the structure deformation induced by the high level of curvature of micelles (*42*), whereas peptides in organic solvent adopt the same structure as in the isotropic planar phospholipid bicelles (*43*). On this basis, both peptides were biologically tested in a medium containing phospholipid membranes which are mimicked in CD and NMR studies by the 50:50 TFE/phosphate buffer medium.

In fact, the U shape of the h-V_{1a} i2 loop is retrieved in the i2 loop of the bovine rhodopsin (Figure 6A). The role of the proline in the bottom base of the U shape seems to be essential since it is conserved in the whole vasopressin receptor family, in rhodopsin and in many other GPCRs. Its crucial role for h-V_2-R structure was further evidenced by Erlenbach et al. (*44*), who demonstrated that the deletion of this Pro residue leads to a loss of binding capacity and functional activity. Pro thus acts as a helix breaker and allows the receptor loop to be folded into a U structure compatible with anchoring to the transmembrane domains. In contrast with those of h-V_{1a}-R or bovine rhodopsin, the i2 loop of the human α2A adrenergic receptor does not contain a proline residue. Its structure, determined by ^{1}H NMR, consists of the succession of three α-helices more or less linearly disposed (*4*). All together, these data suggest that the structures of the GPCR i2 loops exhibit different conformations that are dependent on their sequence and on the presence of a proline residue.

We demonstrate moreover that this proline residue exhibits two conformations in the linear h-V_{1a}-R i2 mimetic peptide. Structure calculations suggest that the Pro11-Leu12 dipeptide presents a crankshaft type conformational equilibrium (*32*−*36*). This equilibrium is local and preserves the global fold of the loop. However, we hypothesize that in the native receptor, its amplitude could be enhanced and trigger a conformational change between activated and inactivated receptor states. Indeed, dynamical simulations show that crankshaft motions can represent the starting step for major conformational changes in proteins (*45*, *46*). The large prevalence of the Pro-Xaa motif (where Xaa represents a

hydrophobic residue) in the second intracellular loop of G protein-coupled receptors suggests that it may be a common mechanism for interaction with G proteins.

The well-formed regular α-helix in the N-terminal part, continuing the TM III helix, represents the last remarkable similarity between the h-V_{1a}-R and rhodopsin cytoplasmic loops. Panels B and C of Figure 6 illustrate the comparison between rhodopsin and h-V_{1a}-R i2 N-terminal helices showing not only global structural similarities but also a comparable hydropathy profile. The biological relevance of a helix in the N-terminal part of the i2 loop was established by mutagenesis studies prior to publication of any structural data for the muscarinic receptor and for the rhodopsin (*37*, *39*). Hence, the rotation of TM III occurring upon ligand binding (*47*) would lead to the rotation of the i2 N-terminal helix as well and constitute the switch enabling G protein activation. Interestingly, the mutation of Asp148 in the DRY motif in the h-V_2-R leads to a constitutively active receptor (*48*), as observed by mutating Glu134 in rhodopsin (*49*).

In summary, the h-V_{1a}-R, which belongs to the rhodopsin GPCR family, possesses a similar i2 structure. In particular, the TM III helices of the vasopressin receptor and rhodopsin extend into cytoplasmic helices with identical hydropathy profiles. Structure analysis underlines the prominent role of the proline residue next to this helix at respective positions 156 and 142 in the common folding. This proline and the adjacent hydrophobic residue are subjected to a conformational equilibrium in the vasopressin receptor linear peptide. This equilibrium could be the sign of a large flexibility of this motif, allowing the easy rotation of the cytoplasmic helix subsequent to rotation of TM III, a process fundamental for interaction of h-V_{1a}-R with G proteins.

ACKNOWLEDGMENT

We thank M. Passama for correction in drawings and M. Chalier and J. Huet for manuscript typing.

SUPPORTING INFORMATION AVAILABLE

^{1}H NMR chemical shifts of i2 lin and i2 cyc peptides, NOESY spectra showing i2 lin Leu12 NH resonances, temperature dependence of the i2 lin line width, folds calculated without long-range NOEs, and NMR spectra for a 10:90 TFE/H_2O mixture at 10 °C. This material is available free of charge via the Internet at http://pubs.acs.org.

REFERENCES

1. Bockaert, J. (1991) *Curr. Opin. Neurobiol. 1*, 32−42.
2. Palczewski, K., Kumasaka, T., Hori, T., Behnke, C. A., Motoshima, H., Fox, B. A., Le Trong, I., Teller, D. C., Okada, T., Stenkamp, R. E., Yamamoto, M., and Miyano, M. (2000) *Science 289*, 739−745.
3. Ballesteros, J. A., Shi, L., and Javitch, J. A. (2001) *Mol. Pharmacol. 60*, 1−19.
4. Chung, D. A., Zuiderweg, E. R. P., Fowler, C. B., Soyer, O. S., Mosberg, H. I., and Neubig, R. R. (2002) *Biochemistry 41*, 3596−3604.
5. Franzoni, L., Nicastro, G., Pertinhez, T. A., Oliveira, E., Nakaie, C. R., Paiva, A. C., Schreier, S., and Spisni, A. (1999) *J. Biol. Chem. 274*, 227−235.
6. Arshava, B., Liu, S.-F., Jiang, H., Breslav, M., Becker, J. M., and Naider, F. (1998) *Biopolymers 46*, 343−357.
7. Pellegrini, M., Royo, M., Chorev, M., and Mierke, D. F. (1996) *Biopolymers 40*, 653−666.
8. Ulfers, A. L., McMurry, J. L., Kendall, D. E., and Mierke, D. F. (2002) *Biochemistry 41*, 11344−11350.
9. Liu, J., and Wess, J. (1996) *J. Biol. Chem. 271*, 8772−8778.
10. Erlenbach, I., and Wess, J. (1998) *J. Biol. Chem. 273*, 26549−26558.
11. Yeagle, P., Choi, G., and Albert, A. D. (2001) *Biochemistry 40*, 11932−11937.
12. Manning, M., Bankowski, K., Barberis, C., Jard, S., Elands, J., and Chan, W. Y. (1992) *Int. J. Pept. Protein Res. 40*, 261−267.
13. Fraker, P. J., and Speck, J. C. (1978) *Biochem. Biophys. Res. Commun. 80*, 849−857.
14. Cotte, N., Balestre, M. N., Phalipou, S., Hibert, M., Manning, M., Barberis, C., and Mouillac, B. (1998) *J. Biol. Chem. 273*, 29462−29468.
15. Jard, S., Gaillard, R. C., Guillon, G., Marie, J., Schanenberg, P., Muller, A. F., Manning, M., and Sawyer, W. H. (1986) *Mol. Pharmacol. 30*, 171−177.
16. Marion, D., Ikura, M., Tshudin, R., and Bax, A. (1989) *J. Magn. Reson. 85*, 393−399.
17. Kadkhodaei, M., Hwang, T. L., and Shaka, A. J. (1993) *J. Magn. Reson., Ser. A 105*, 105−107.
18. Piotto, M., Saudek, V., and Sklenar, V. (1992) *J. Biomol. NMR 2*, 661−665.
19. Pons, J. M., Malliavin, T. E., and Delsuc, M. A. (1996) *J. Biomol. NMR 8*, 445−452.
20. Linge, J. P., O'Donoghue, S. I., and Nilges, M. (2001) *Methods Enzymol. 339*, 71−90.
21. Brunger, A. T., Adams, P. D., Clore, G. M., DeLano, W. L., Gros, P., Grosse-Kunstleve, R. W., Jiang, J. S., Kuszewski, J., Nilges, M., Pannu, N. S., Read, R. J., Rice, L. M., Simonson, T., and Warren, G. L. (1998) *Acta Crystallogr. D54*, 905−921.
22. Phalipou, S., Seyer, R., Cotte, N., Breton, C., Barberis, C., Hibert, M., and Mouillac, B. (1999) *J. Biol. Chem. 274*, 23316−23327.
23. Englebretsen, D. R., Choma, C. T., and Robillard, G. T. (1998) *Tetrahedron Lett. 39*, 4929−4932.
24. König, B., Arendt, A., McDowell, J. H., Kahlert, M., Hargrave, P. A., and Hofmann, K. P. (1989) *Proc. Natl. Acad. Sci. U.S.A. 86*, 6878−6882.
25. Dalman, H. M., and Neubig, R. R. (1991) *J. Biol. Chem. 266*, 11025−11029.
26. König, B., and Grätzel, M. (1994) *Biochim. Biophys. Acta 1223*, 261−266.
27. Varrault, A., Le Nguyen, D., McClue, S., Harris, B., Jouin, P., and Bockaert, J. (1994) *J. Biol. Chem. 269*, 16720−16725.
28. Mendre, C., Dufour, M. N., Le Roux, S., Seyer, R., Guillou, L., Calas, B., and Guillon, G. (1997) *J. Biol. Chem. 272*, 21027−21036.
29. Hebert, T. E., Moffet, S., Morello, J. P., Loisel, T. P., Bichet, D. G., Barret, C., and Bouvier, M. (1996) *J. Biol. Chem. 271*, 16384−16392.
30. Wüthrich, K. (1986) *NMR of Proteins and Nucleic Acids*, John Wiley and Sons, New York.
31. Wishart, D. S., Sykes, B. D., and Richards, F. M. (1992) *Biochemistry 31*, 1647−1651.
32. MacCammon, J. A., Gelin, B. R., Karplus, M., and Wolynes, P. G. (1976) *Nature 262*, 325−326.
33. Levitt, M. (1983) *J. Mol. Biol. 168*, 621−657.
34. Chandrasekhar, I., Clore, G. M., Szabo, A., Gronenborn, A. M., and Brooks, B. R. (1992) *J. Mol. Biol. 226*, 239−250.
35. Wasserman, Z. R., and Salemme, F. R. (1990) *Biopolymers 29*, 1613−1631.
36. Fadel, A. R., Jin, D. Q., Montelione, G. T., and Levy, R. M. (1995) *J. Biomol. NMR 6*, 221−226.
37. Burstein, E. S., Spalding, T. A., and Brann, M. R. (1998) *J. Biol. Chem. 273*, 24322−24327.
38. Moro, O., Lameh, J., Högger, P., and Sadée, W. (1993) *J. Biol. Chem. 268*, 22273−22276.
39. Yamashita, T., Terakita, A., and Shichida, Y. (2000) *J. Biol. Chem. 275*, 34272−34279.
40. Yeagle, P. L., Alderfer, J. L., Salloum, A. C., Ali, L., and Albert, A. D. (1997) *Biochemistry 36*, 3864−3869.
41. Yeagle, P. L., Alderfer, J. L., and Albert, A. D. (1997) *Biochemistry 36*, 9649−9654.
42. Chou, J. J., Kaufman, J. D., Stahl, S. J., Wingfield, P. T., and Bax, A. (2002) *J. Am. Chem. Soc. 124*, 2450−2451.
43. Andersson, A., and Maler, L. (2002) *J. Biomol. NMR 24*, 103−112.

44. Erlenbach, I., Kostenis, E., Schmidt, C., Serradeil-Le Gal, C., Raufaste, D., Dumont, M. E., Pausch, M. H., and Wess, J. (2001) *J. Biol. Chem. 276*, 29382−29392.
45. Philippopoulos, M., Xiang, Y., and Lim, C. (1995) *Protein Eng. 8*, 565−573.
46. Berjanskii, M. V., Riley, M. I., and Van Doren, S. R. (2002) *J. Mol. Biol. 321*, 503−516.
47. Gether, U., Lin, S., Ghanouni, P., Ballesteros, J. A., Weinstein, H., and Kobilka, B. K. (1997) *EMBO J. 16*, 6737−6747.
48. Morin, D., Cotte, N., Balestre, M. N., Mouillac, B., Manning, M., Breton, C., and Barberis, C. (1998) *FEBS Lett. 441*, 470−475.
49. Kim, J. M., Altenbach, C., Thurmond, R. L., Khorana, H. G., and Hubell, W. L. (1997) *Proc. Natl. Acad. Sci. U.S.A. 94*, 14273−14278.
50. Laskowski, R. A., MacArthur, M. W., Moss, D. S., and Thorton, J. M. (1993) *J. Appl. Crystallogr. 26*, 283−291.

BI027358N